Low Speed Take-Off Aerodynamic Analysis

D. Charbonnier & J.B. Vos
CFS Engineering
EPFL Innovation Park, Batiment A, 1015 Lausanne, Switzerland

P.S. Prakasha
German Aerospace Center (DLR),
Institute of System Architectures in Aeronautics, Hein-Sassweg 22, 21129 Hamburg, Germany

A. Mirzoyan
Central Institute of Aviation Motors (CIAM), Aviamotornays Str. 2, 111116 Moscow, Russia

A. Savelyev
Propulsion Systems Aero Department, TsAGI, Zhukovskiy 1, 140180 Moscow Oblast, Russia

P. Della Vecchia
Dept. of Industrial Engineering, University of Naples "Federico II", Via Claudiao 21, 80125 Napoli, Italy

ABSTRACT

In the frame of the EU funded H2020 project AGILE (Aircraft 3rd Generation MDO for Innovative Collaboration of Heterogeneous Teams of Experts) detailed CFD simulations were made to analyze the high lift system of an optimized regional aircraft. The paper presents shortly how the different components of the aircraft were obtained and integrated in a model suitable to perform the simulations. High-fidelity RANS (Reynolds-Averaged Navier-Stokes) CFD calculations were carried out, with a focus on take-off conditions, and aerodynamic coefficients as well as flow field distributions were extracted. The results are discussed, and point out in one hand the reliability of high-fidelity CFD simulations to highlight detailed flow phenomena like flow separations, and in another hand the importance to consider low speed flow regimes (take-off or landing) in an aircraft design and optimization process.

KEYWORDS: MDO, CFD, High-Lift

1. INTRODUCTION

Aircraft multidisciplinary optimization is a highly complex process requiring the involvement of a large number of specialists from a wide range of disciplines. Each of these specialist use their own tools, and these tools often have different levels of fidelity (= representation of the physics involved).
Tradionally the aircraft design process is divided into 3 phases, the Conceptual, the Preliminary and the Detailed Design. In the Conceptual Design phase many variants need to be studied and a fast turn around time of the tools being used is important. This means that mainly low fidelity tools are used in this phase, having the risk that this leads to flaws in the design requiring costly redesign at later stages in the design process.
Since the middle of 1990's efforts are underway to increase the fidelity of the tools being used in the Conceptual Design phase through the so called 'Virtual Product' that was defined as a 'high-fidelity mathematical/numerical representation of the physical properties and the functions of a product' [1, 2]. Critical to the success of the 'Virtual Product' is the capability for rapid generation of high-fidelity information from all disciplines involved, and the implementation of new multidisciplanary simulation and optimization environments [3].
Aircraft development programs are today organized as collaborative and multi-organizational processes. A major challenge hampering a cost effective design is the integration of multidisciplinary competences in the so called 'Virtual Entreprise'. The challenge becomes even larger when the required competences are provided by heterogeneous teams of specialists distributed in different organizations and across nations. This requires new Multi-disciplinary Design Optimization (MDO) methodologies using a standard approach and interface for communication between disciplinary modules.
The AGILE (Aircraft 3rd Generation MDO for Innovative Collaboration of Heterogeneous Teams of Experts) Horizon 2020 funded project is developing and implementing the next generation of aircraft MDO processes

targeting a reduction of 20% in time to converge the design of an aircraft and a 40% reduction in time needed to setup and solve the MDO problem using a team of heterogeneous specialists.
The AGILE project involves a team of 19 industry, research and academia partners from Europe, Canada and Russia. The AGILE project has formulated the so called 'AGILE Paradigm' [4] accelerating the deployment of collaborative, large scale design and optimization frameworks, and in particular (as shown in Fig. 1):

- Accelerating the setup and deployment of distributed, cross-organizational MDO processes
- Supporting the collaborative operation of design systems: integrating people and tools
- Exploiting the potential offered by the latest technologies in collaborative design and optimization

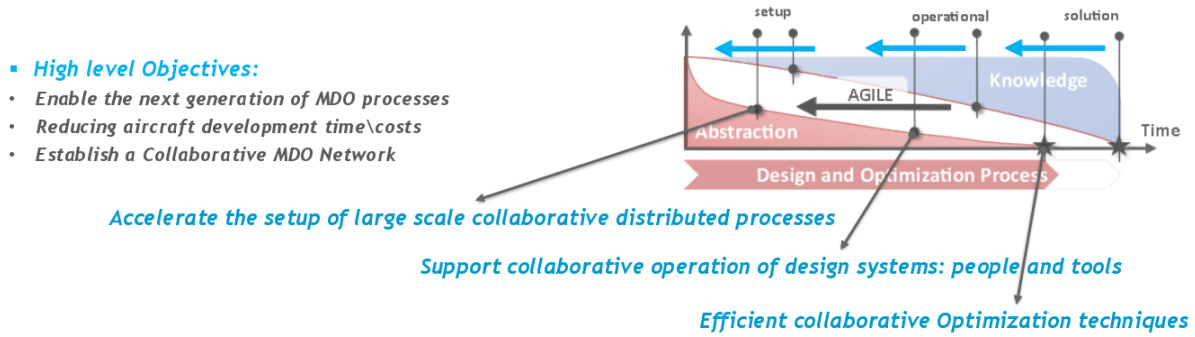

Figure 1: AGILE 3rd Generation Design and Optimization Processes.

The main elements of the AGILE Paradigm are the Knowledge Architecture (formalization of the product development process as a hierarchical structures process) and the Collaborative Architecture (enables cross-organizational and cross national integration of distributed design competences of the project partners) [4]. In AGILE the MDO activities are undertaken in 3 sequential work packages, targeting design cases with increasing level of complexity and addressing different aircraft configurations.
The work presented in this paper is concerned with the so-called Design Campaign-2 (DC-2) that was carried out in the 2nd year of the AGILE project [5]. The reference aircraft in this design campaign, coming from the DC-1 campaign, is a regional civil aircraft with the top level aircraft requirements summarized in Table 1 and the aircraft (before optimization) is shown in Fig. 2.

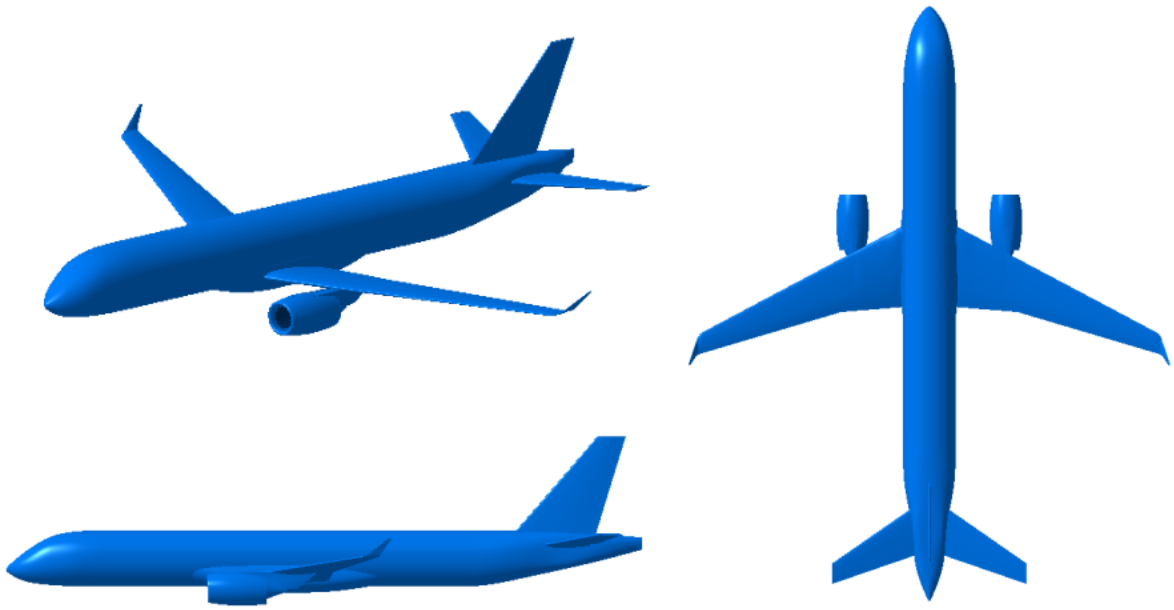

Figure 2: Starting point AGILE Design Campaing 2 aircraft.

Conventional Large Regional Jet Reference Aircraft (EIS: 2020)		
	Metric	***Imperial***
Range	3500 km	1890 nm
Design payload	9180 kg	20220 lbs
Max. payload	11500 kg	25330 lbs
PAX	90 pax @ 102 kg	90 pax @ 225 lbs
MLW (% MTOW)	90%	
Long Range Cruise Mach (LRC)	0.78	0.78
Initial Climb Altitude (ICA)	11000 m	36000 ft
Maximum Operating Altitude	12500 m	41000 ft
Residual climb rate	91 m/min	300 ft/min
TOFL (ISA, SL, MTOW)	1500 m	4921 ft
Vref (ISA, SL, MLW)	< 130 kts	
Max. operation speed (V_{mo} / M_{mo})	330 KCAS / 0.82	
Dive Mach number (M_d)	0.89	
Fuselage diameter	3 m	118 in
Fuselage length	34 m	111.5 ft
Service life	80,000 cycles	
Fuel reserves	5%	100 nm
A/C configuration	Low-wing, wing-mounted engines	
Engine	Provided (e.g.: PW1700G)	
Design objective	Minimize COC (alternatively, min. MTOW)	

Table 1: AGILE DC-2 Top Level Aircraft Requirements.

In DC-2 several different optimization studies were carried out by different teams. For example the Nacelle design was optimized using 18 different design variables [5]. The wing was optimized in DC-1 with preliminary high-lift device and medium fidelity aero-structure analysis helped to find the optimum configuration of the wing. This is the phase where a large design space is explored and reduced to one optimum which is DC2- aircraft [6]. The optimized wing and nacelle, together with the high-lift system were put together and a detailed high fidelity analysis was made studying the Take-off behaviour of the aircraft. The results of this study is presented in this paper. In section 2 the different components of the DC-2 aircraft used in this study are discussed. Section 3 discussed the grid generation and numerical set-up. Section 4 discussed the results obtained.

2. AGILE MULTI-DISCIPLINARY INTEGRATION

Figure 3 shows the Multi Disciplinary Optimization integration flow chart. The starting point are the Top Level Aircraft Requirements (TLAR) used in Design Campaign-2, see also Table 1, and further details can be found in [8].

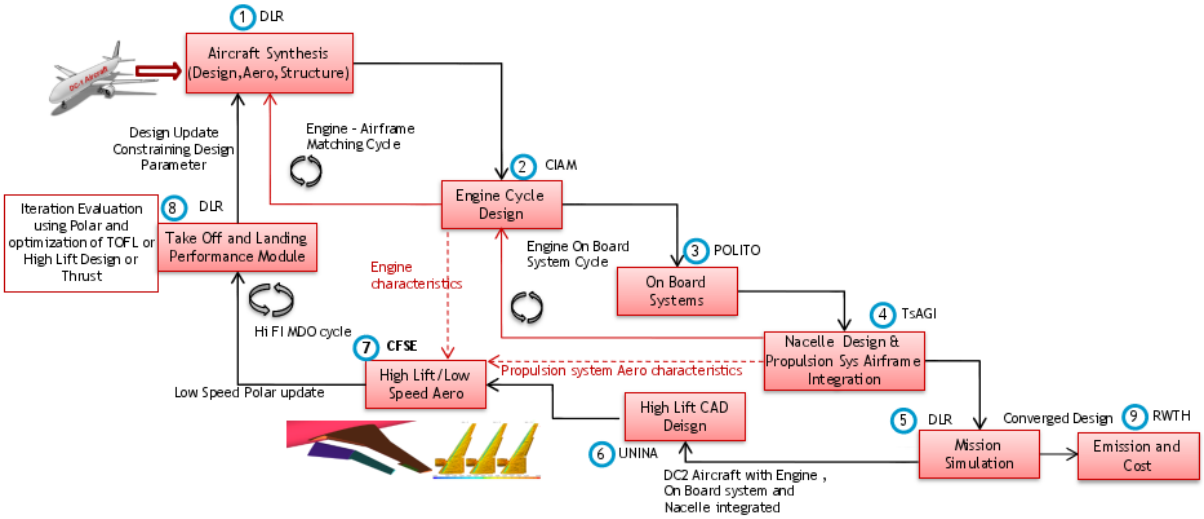

Figure 3: AGILE DC2 High Fidelity Multi-Disciplinary Optimization Integration Flowchart.

The MDO integration flowchart and AGILE partner involvement is as follows:

1. DLR : Initial synthesis based on requirements and Medium Fidelity Aero-Structure analysis is performed

2. CIAM: Based on Thrust requirements and Engine is designed through an iterative Engine-Airframe design matching cycle

3. POLITO: On Board System (OBS) is designed based on the TLAR, Cabin comfort and OBS architectural requirements (more electric or all electric or conventional) and weight and power offtakes are evaluated. Further OBS effect on Engine offtakes are considered in Engine-Onboard system cycle.

4. TsAGI: The Engine parameters are considered for nacelle design and integrated on the airframe. The propulsion system integration and aerodynamic optimization is performed at this point.

5. DLR: Mission simulation is performed with updated Weights, Aerodynamics and Engine performance, Fuel estimations are made. But these are based on High Fidelity cruise aerodynamic optimization. High fidelity low speed aerodynamics was desired for evaluating correct thrust and take off performance

6. UNINA: High Lift system design and CAD geometry generation to permit High Fidelity low speed aerodynamics evaluation

7. CFSE: Low speed aero performance was evaluated, and this is the focus of the current paper

8. DLR: Take Off and Landing Analysis will be performed using the updated Drag polars for the low speed regime and design optimization iteration with respect to High lift device, Engine Thrust (installed), Take off field length will be made. A tradeoff analysis.
   DLR: Go back to step 1: and a second iteration for design optimization is started

9. RWTH: The converged design is evaluated for emission characteristics and life cycle cost. The fuel efficiency is the primary objective function, hence the cost and emission is not inside optimization loop.

Note : The focus of this paper is on Step 7. The results obtained from Step 7 will be used in steps 8,9 for optimization, as well as in steps 4 and 5 to re-investigate the nacelle position and the high-lift system design. Which will be updated and presented in a next publication.

3. MODEL SETUP

Several components of the DC2-aircraft (geometrical components or computational parameters) were taken from other sub-tasks of the AGILE project related to the creation of a 3D model suitable for high fidelity aerodynamic analysis, see also sections 3 and 4. These components are shortly discussed in the following subsections, namely:

- Nacelle design
- Engine deck
- High-lift devices

3.1. Nacelle design

TsAGI performed the aerodynamic optimization of the propulsion system of the DC-2 aircraft. This task included the optimization of the isolated nacelle, the nacelle positioning and the positioning of the pylon [9]. For the optimization, TsAGI used the engine deck provided by CIAM and the DC-2 airframe from DLR. The optimization was performed at cruise regime. As result TsAGI returned the geometry of nacelle and pylon, the drag and lift coefficients for the full configuration and for each of the elements separately.
The initial nacelle design used in the optimization was also provided by TsAGI. For the optimization all processes were integrated into one analysis workflow using the RCE environment [10], shown in Fig. 4a. The figure shows that the workflow consists of five tasks: CPACS [11] file reading, CPACS converting into internal formats, aerodynamic analysis, converting and writing a new CPACS file with the results. The aerodynamic analysis block includes geometry construction, meshing, CFD calculation and post-processing. For the CFD calculations, TsAGI uses the Electronic Wind Tunnel (EWT) in-house solver [12]. This aerodynamic analysis block is used for nacelle optimization procedure. When the isolated nacelle optimization is finished, the nacelle position optimization is started. During this part of the optimization the nacelle position is modified as shown in Fig. 4b. In a first phase, only the initial nacelle design and the installation angles are used for the wing optimization task.

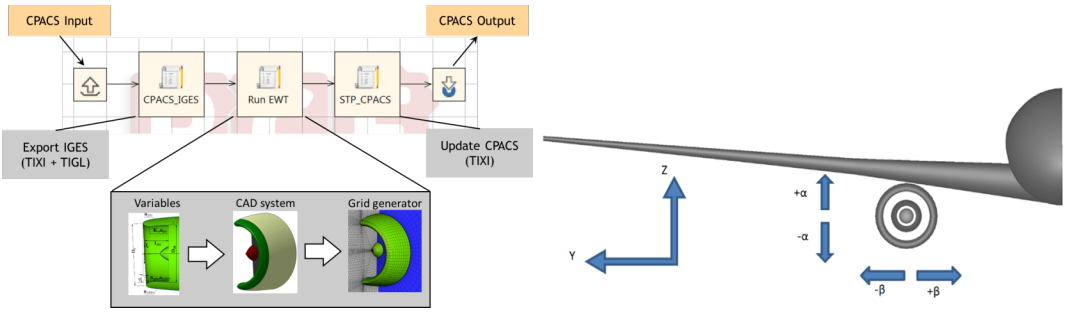

(a) Design analysis workflow (b) Position optimization

Figure 4: Nacelle design.

3.2. Engine deck

To generate the Engine Deck (ED), the commercial software tool GasTurb v12 for engine modeling was used by CIAM. This tool corresponds to an engine simulation using empirical methods of engine components (compressors, turbines, combustor, etc.), i.e. 'black boxes' without detailed (1D-3D) modeling. The GasTurb tool was used to evaluate the on-design and off-design engine parameters and the performance map. The engine component maps are presented in the engine tool using specific components maps. Engine model technology constraints and design rules are used in engine cycle design, off-design simulation and engine overall geometry and mass assessments. Technology constraints and design rules were applied to generate an ED consistent with the specified technology. More details about the engine simulation tool are given in [13, 14].

The following engine data were added to the CPACS file for their use in the Low speed aerodynamic CFD simulation: Engine installed thrust FN, fan inlet total pressure and temperature (station 2) Pt2 and Tt2, engine corrected mass flow rate (station 2) wDot2R, fan bypass exit total pressure and temperature (station 13)

Pt13 and Tt13, fan bypass exit mass flow rate (station 13) wDot13, core exit total pressure and temperature (station 5) Pt5 and Tt5, core exit mass flow rate (station 5) wDot5. The engine stations are shown in Fig. 5a.

All these engine data are calculated for Max TakeOff (MTO) flight conditions at Mach numbers M_{MTO} 0.20, 0.25 and 0.30. The M_{MTO} has a significant influence on the engine parameters as can be seen in Fig. 5b. For example, the Thrust FN is reduced by 25% when increasing M_{MTO} from 0 to 0.3, and the fan bypass exit massflow rate (wDot13) is increased by 11%.

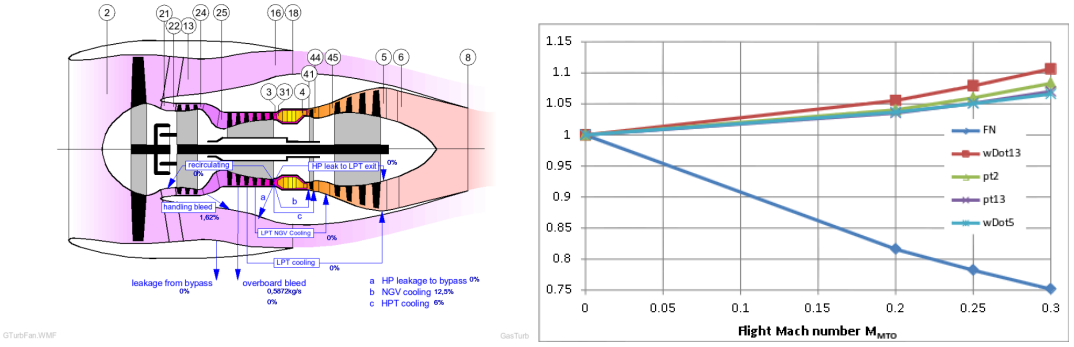

(a) Identification of Engine Stations

(b) Influence of flight Mach number M_{MTO} on the main engine parameters

Figure 5: Engine deck.

3.3. High-Lift devices

The University of Naples (UNINA) has worked on the design of a high fidelity CAD model for the wing of the DC-2 aircraft including the high-lift movables. The flap design follows this procedure: starting from the optimized reference wing of the DC-2 aircraft, a semiempirical approach allows to choose the high-lift device type(slot, fowler, etc), the right chord extensions, span and deflections, to be compliant to top level aircraft requirements (see Table 1). Then an automated procedure allow to design the 3D geometry, cutting opportunely the wing, imposing the above computed parameters (see Fig. 6).

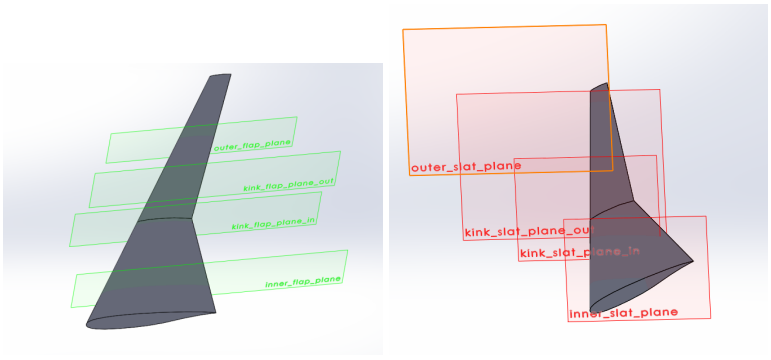

(a) flap

(b) slat

Figure 6: Cutting plane for high-lift device design on wing

A fowler flap and a leading edge slat have been chosen and designed at reference sections in a CAD environment, and then analysed and optimized one by one. A 2-dimensional aerodynamic analysis has been performed on two reference airfoils (one on the inner section and the other on the outer section), in order to define the better values for gap and overlap for both take-off and landing configurations. A genetic algorithm optimization procedure, performing on aerodynamic maps on both take-off and landing configurations (on an objective function which takes into account for CImax, Cd@alpha=0, Cl0 and Clalpha), leads to optimized multi-elements airfoil whose gap and ovelap parameters have been employed to design the 3D CAD geometry. Based on 2D aerodynamic analyses and optimization, the 3D CAD (normal take-off, take-off and landind), including the optimized nacelle and pylon geometries provided by TsAGI, has been generated and provided

to partners.
In the present study, the high-lift components have been deflected for two flight configurations: landing and take-off, and exported in a CAD file suitable for mesh generation for CFD aerodynamic analysis. The design of the aircraft wing including the high-lift devices is shown in Fig. 7. For the landing configuration, the slat (both inner and outer) is deflected by 25° while the flap is deflected by 35° (Fig. 7b), and for the take-off configuration the slat and the flap are both deflected by 20° (Fig. 7c).

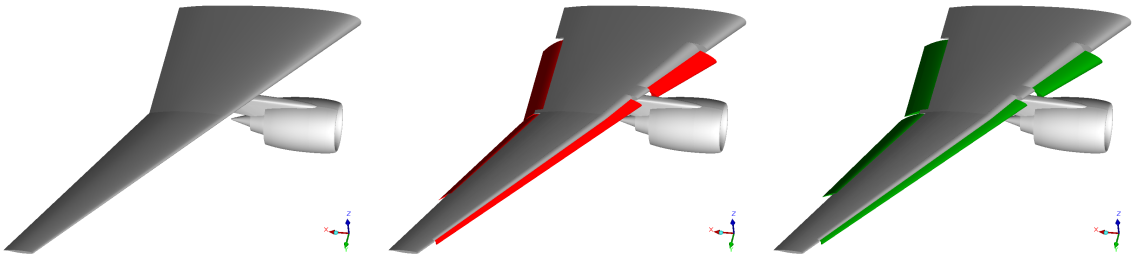

(a) clean (b) landing (c) take-off

Figure 7: Wing configurations with or without deflected high-lift devices.

4. NUMERICAL SETUP

All the aircraft components from the different partners (DLR, UNINA, TsAGI, CIAM), described in section 3, were merged together in a 3D model suitable for the mesh generation process and high fidelity CFD aerodynamic simulations. The DC2-aircraft model is shown in Fig.8. The picture shows the input components with their formats (CPACS or CAD files) and the final 3D model after assembly. One can note that the pylon was removed on the final assembly. As a first approximation, in order to simplify the meshing process, it was decided to remove this part. However a small study was performed on a coarse grid, and the drag and lift coefficients were increased by 4% and 1% respectively for the case with the pylon.

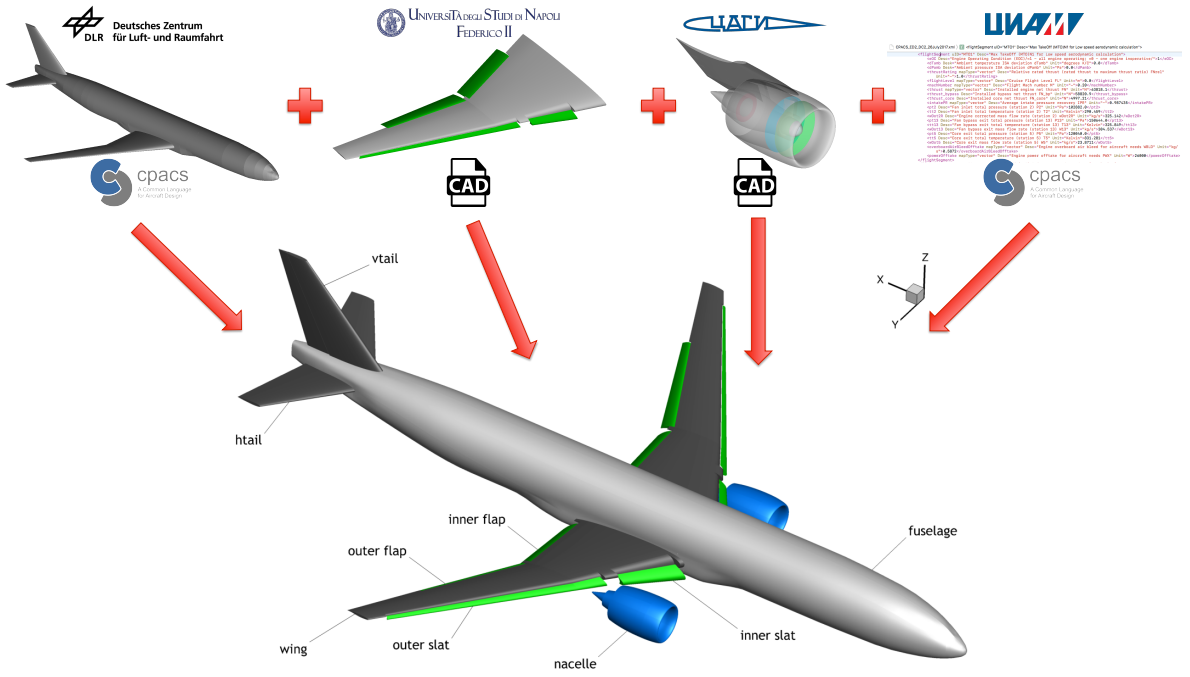

Figure 8: DC2-aircraft model for CFD aerodynamic analysis.

4.1. Grid generation

The ANSYS® ICEM CFD™ pre-processer tool was used to generate the multi-block structured grids needed by the Navier-Stokes Multi-Block flow solver NSMB. The grid topology was always generated for a half configuration, and a copy by mirror was applied for full configuration, if required for the case computed (rudder effect, one engine off effect,...) which was not the case in the analysis presented in this study, but in other tasks of the project. The grid was designed using the chimera method in order to simplify the mesh generation process and to generate quickly multiple configurations with different deflections of the control surfaces (high-lift devices on the wing as well as the rudder on the vertical tail), or to optimize the position of the nacelle. To resolve the viscous boundary layer an O-grid topology with a geometric cell distribution was used around the solid walls. The first cell height in the wall normal direction was set to obtain a y+ value close to/below 1 to ensure the proper use of low-Reynolds turbulence modeling, and the growth ratio of the cells normal to the wall was typically close to 1.2.

The grid topology is made of 787 structured blocks, including 471 blocks for the main grid (fuselage, wing, horizontal tail and vertical tail), 229 blocks for the overlapping grid of the nacelle and finally 87 chimera blocks around the high-lift devices (inner slat, outer slat, inner flap and outer flap). In terms of number of cells, the grid for the half configuration comprises 23.3 Million cells, with respectively 17.9 Million, 3.3 Million and 2.1 Million for the airframe, the nacelle and the high-lift devices. Detailed views of the mesh are shown in Fig. 9. One can see the overlapping grids after blanking process on Fig. 9d and 9e, in blue for the nacelle and in green for the movable devices. Thanks to the chimera method, the displacement of the movables is straight-forward, without any remeshing process, as highlighted in Fig. 9e for two configurations at take-off conditions (fully or partially deployed).

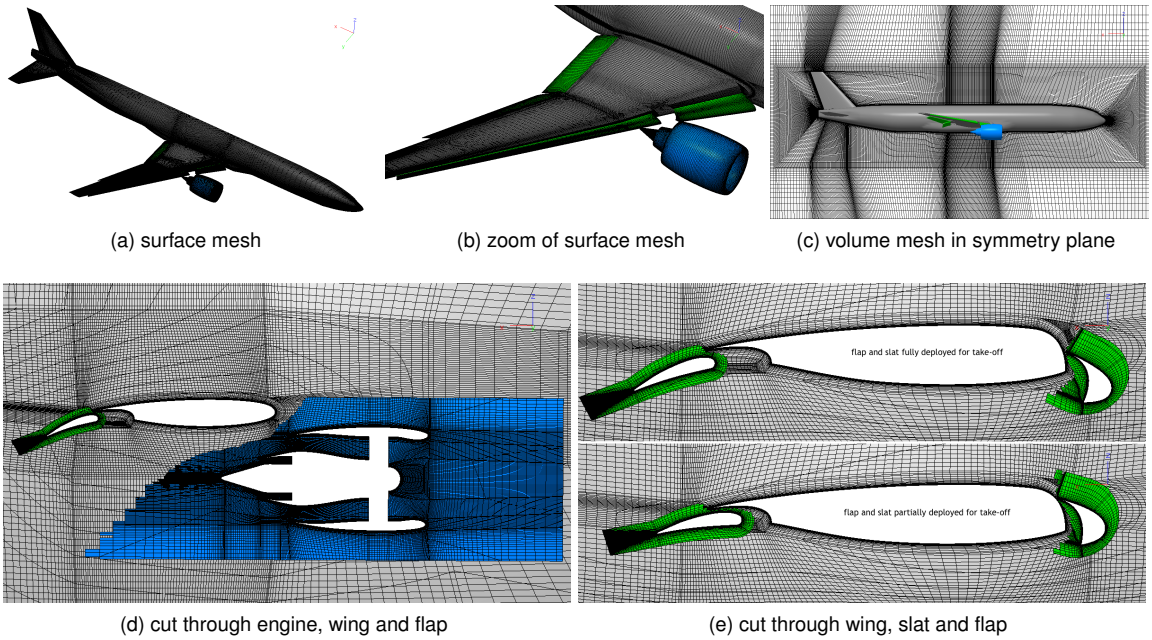

(a) surface mesh (b) zoom of surface mesh (c) volume mesh in symmetry plane

(d) cut through engine, wing and flap (e) cut through wing, slat and flap

Figure 9: DC2-aircraft Chimera grid.

4.2. Computational setup

4.2.1. Computational code

All calculations were made using the NSMB solver. NSMB was initially developed in 1992 at the Swiss Federal Institute of Technology (EPFL) in Lausanne, and from 1993 onwards in the NSMB consortium composed of different universities, research establishments and industries. Today NSMB is developed by IMF-Toulouse (IMF Toulouse, France), ICUBE (Strasbourg, France), University of Munchen (TUM, Germany), University of the Army in Munchen (Germany), Airbus Safran (France), RUAG Aviation and CFS Engineering. A variety of papers have been published on NSMB, some examples are in [15–17]
NSMB is a CFD solver using the cell-centered finite volume method on multi block structured grids. To simplify the mesh generation for complex geometries NSMB uses the patch grid (also known as the sliding mesh) approach and the chimera method.
Space discretization schemes implemented in NSMB are the 2^{nd} and 4^{th} order central schemes with artificial dissipation and Roe and AUSM upwind schemes from 1^{st} to 5^{th} order. Time integration can be made using explicit Runge-Kutta schemes, or the semi-implicit LU-SGS scheme. Different methods have been implemented to accelerate the convergence to steady state, as for example local time stepping, multigrid and full multigrid, and low Mach number preconditioning. Unsteady simulations are made using the dual time stepping approach or using the 3rd order Runge Kutta scheme.
Turbulence is modelled using standard approaches as for example the algebraic Baldwin-Lomax model, the 1-equation Spalart model (and several of it's variants) and the $k-\omega$ family of models (including the Wilcox and Menter Shear Stress models). Explicit Algebraic Reynolds Stress models and Reynolds Stress models have also been implemented, but are not used on a routine base. Transition to turbulence can be modelled by specifying transition lines or planes, or by solving the $\gamma - R_\theta$ transport equations [18]. For unsteady CFD simulations different Hybrid RANS-LES models are available.

4.2.2. Computational matrix

A first set of 15 calculations were made on the configuration with fully deployed high-lift devices (Fig. 9e top) varying the angle of attack and Mach number. Based on the results of these calculations, see Section 5 and additional 6 calculations were made on the configuration with partially deployed movables (Fig. 9e bottom). The entire computational matrix for these 21 calculations is given in Table 2. All the calculations were performed using the 2^{nd}-order Roe upwind space discretization scheme and the LU-SGS time integration scheme. Local time stepping was employed to accelerate the convergence to steady state. A fully turbulent flow was assumed, and the turbulence was modelled using the $k-\omega$ Menter Shear Stress model. The engine

conditions, extracted from the Engine Deck (see section 3.2), were imposed at the boundary conditions of the nacelle, i.e. fan inlet, fan outlet and core outlet. The precise conditions are also given in Table 2.

Flight conditions		Flow conditions					Engine conditions					
configuration	high-lift devices	Mach	AoA	Alt	Re [/m]	Turbulence model	Fan_in Pt	Fan_in Tt	Fan_out Pt	Fan_out Tt	Core_out Pt	Core_out Tt
take-off	fully deployed	0.2	5, 7, 9, 11, 13	0	4.66E+6	$k-\omega$ MSS	102882	290.46	150644	325.85	120040	831.28
		0.25			5.88E+6		104803	291.76	152941	326.92	120632	829.65
		0.3			6.99E+6		107120	293.34	155705	328.26	121157	827.68
	partially deployed	0.25	5, 9, 13	0	5.88E+6	$k-\omega$ MSS	104803	291.76	152941	326.92	120632	829.65
		0.3			6.99E+6		107120	293.34	155705	328.26	121157	827.68

Table 2: Computational matrix.

5. NUMERICAL RESULTS

Figure 10 shows the Mach number contours in a cutting plane through the engine. The case shown here is for the Mach number of 0.25 and the angle of attack 9^o; the behavior is similar for all other cases. The figure highlights the engine jet downstream of the nacelle and the good continuity of the flow through the chimera boundaries.

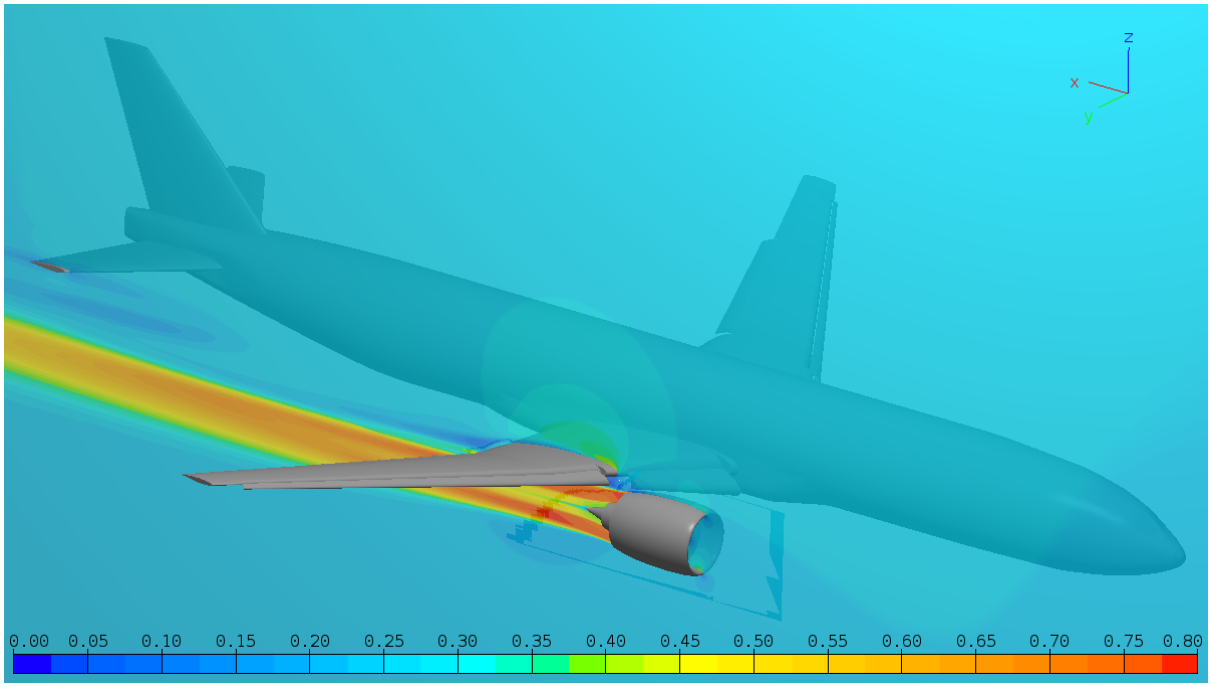

Figure 10: Mach number distribution in a cutting plane through the engine at Mach=0.25.

Table 3 summarizes the computed aerodynamic coefficients (drag coefficient C_D, lift coefficient C_L, pitching moment coefficient Cm), the aerodynamic forces (drag D, lift L) as well as the lift over drag ratio L/D of the 21 calculations. The aerodynamic coefficients were calculated using the reference length $C_{ref} = 3.541812$, the reference surface $S_{ref} = 75$ and the moment reduction centre $XYZ_{ref} = (15.6949, 0.0, 0.0)$ (with the origin at the nose of the aircraft). The results are for a half configuration aircraft, just as the thrust which concerns a single engine. These data are plotted on the curves in Fig. 11 as function of angle of attack, using different colors for different Mach numbers. The cases with fully deployed high-lift devices are depicted with solid lines, while the cases with the partially deployed movables are depicted with dashed lines. On Fig. 11e the engine thrust (depending on the Mach number considered) is also shown using dotted lines.
Figures 11a and 11b show what was to be expected, increasing the Mach number mostly influences the drag coefficient, leading to a lower C_D. This is mostly due to the fact that the dynamic pressure increases more rapidly with the Mach number than the drag force, see Fig. 11e. The lift coefficient shows that stall occurs between angles of attack between 11^o and 13^o for the fully deployed high lift system. No results at an angle of attack of 11^o are available for the partially deployed high lift system. Deploying the high lift system only partially results in a considerable lower lift and drag force.
Figure 11e compares the computed drag force with the thrust provided by the engine. When using the fully

Case	Mach	AoA	Thrust [N]	CD [-]	CL [-]	Cm [-]	D [N]	L [N]	L/D [-]
Take-off fully deployed	0.2	5	63818	0.2029	1.3638	-0.7736	21583	145092	6.7227
		7		0.2322	1.5707	-0.8241	24708	167113	6.7634
		9		0.2639	1.7788	-0.8870	28077	189251	6.7405
		11		0.2997	1.9627	-0.9757	31886	208814	6.5489
		13		0.3499	1.8456	-0.9899	37224	196356	5.2750
	0.25	5	61169	0.1780	1.3733	-0.7706	29593	228299	7.7145
		7		0.2075	1.5809	-0.8165	34494	262796	7.6186
		9		0.2400	1.7947	-0.9096	39903	298351	7.4768
		11		0.2762	1.9464	-0.9454	45911	323556	7.0474
		13		0.3217	1.8010	-0.9781	53478	299398	5.5985
	0.3	5	58792	0.1643	1.3812	-0.7674	39325	330632	8.4076
		7		0.1943	1.5951	-0.8268	46516	381831	8.2085
		9		0.2259	1.7942	-0.8758	54066	429487	7.9437
		11		0.2641	1.9594	-0.9402	63216	469047	7.4198
		13		0.3049	1.7524	-0.9473	72992	419481	5.7470
Take-Off partially deployed	0.25	5	61169	0.1271	1.0090	-0.5426	21125	167729	7.9397
		9		0.1814	1.2238	-0.6020	30162	203433	6.7447
		13		0.2490	1.4431	-0.7254	41390	239889	5.7959
	0.3	5	58792	0.1146	1.0248	-0.5436	27443	245327	8.9396
		9		0.1626	1.3479	-0.6377	38914	322651	8.2915
		13		0.2379	1.4514	-0.7729	56958	347437	6.0999

Table 3: Aerodynamic coefficients and forces.

deployed high lift system one can see that for the Mach=0.3 case the thrust is lower than the drag at angles of attack of 11^o and 13^o. Partially deploying the high lift system solves this problem, but in this case the lift force is substantially lower, resulting in a lower climb rate. One should note that the typical take off speed of commercial aircraft are between Mach=0.20 and Mach=0.25, and that take-off in general takes place with an angle of attack between 7^o and 11^o [19].

Figure 12 shows the pressure distribution on the wing, the movables (inner slat, outer slat, inner flap and outer flap) and the nacelle, as well as the skin friction lines for the three highest angle of attack, for the selected Mach number of 0.25. The skin friction lines permits to highlight the separated flow area that occurs on the suction side of the wing downstream of the nacelle location at angle of attack 13°. This explains the behavior of the lift coefficient and lift force curves (Fig. 11b,11f) with a decrease of the lift when increasing the angle of attack over 11°. One can also observe that for these 3 angles of attack there is small flow separation on the wing tip.

The flow separation at the wing tip was further investigated, and Fig. 13 shows the calculated pressure contours and skin friction lines for the calculations with angles of attack of 5^o and 7^o and for the Mach numbers of 0.20 and 0.25. One can clearly observe that for the angle of attack of 5^o there seems to be a small flow separation that seems to come from the gap between wing and slat. This flow separation has substantially grown for the angle of attack of 7^o. The origin for this is that the tip twist angle is too low because the wing optimization process did not account for the load distribution.

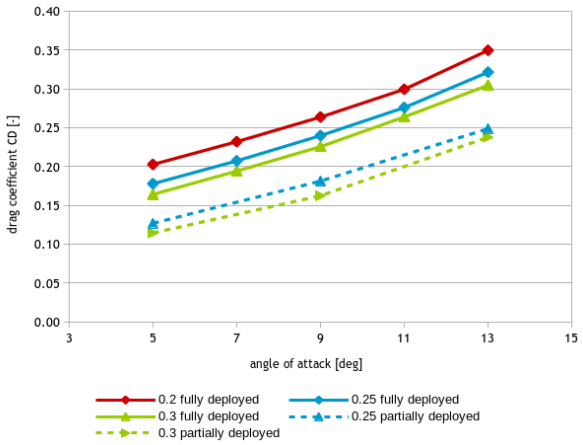

(a) Drag coefficient

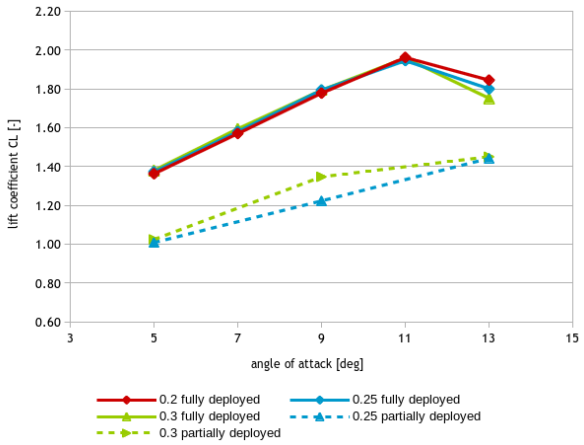

(b) Lift coefficient

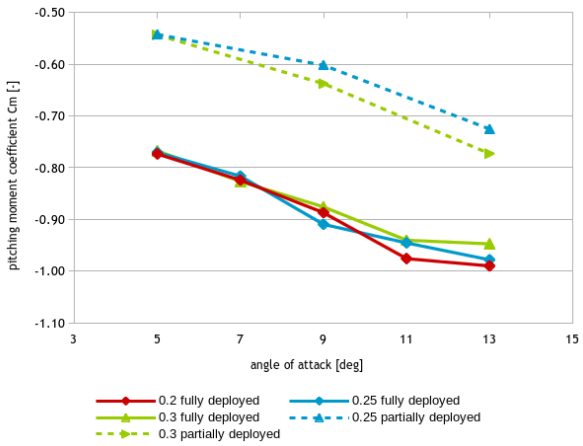

(c) Pitching moment coefficient

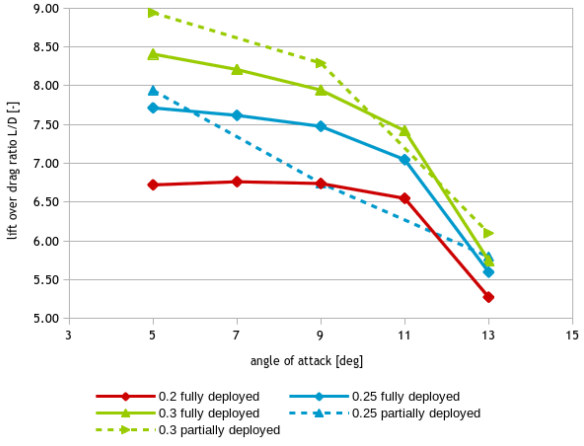

(d) Lift over drag ratio

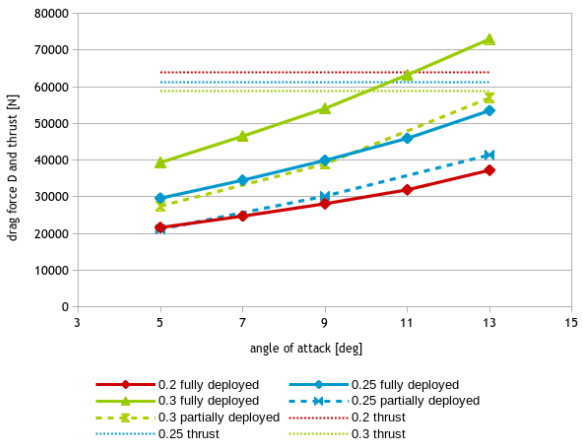

(e) Drag force and thrust

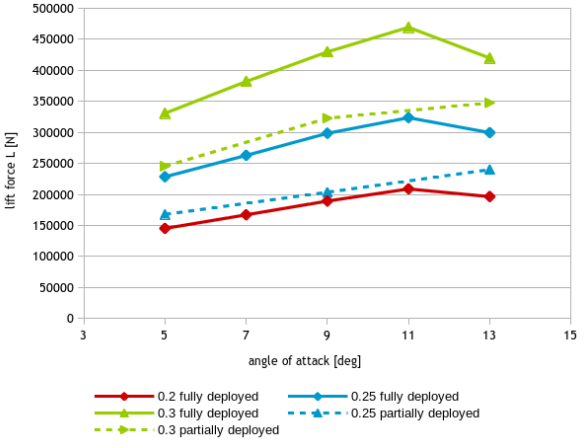

(f) Lift force

Figure 11: Aerodynamic coefficients and forces.

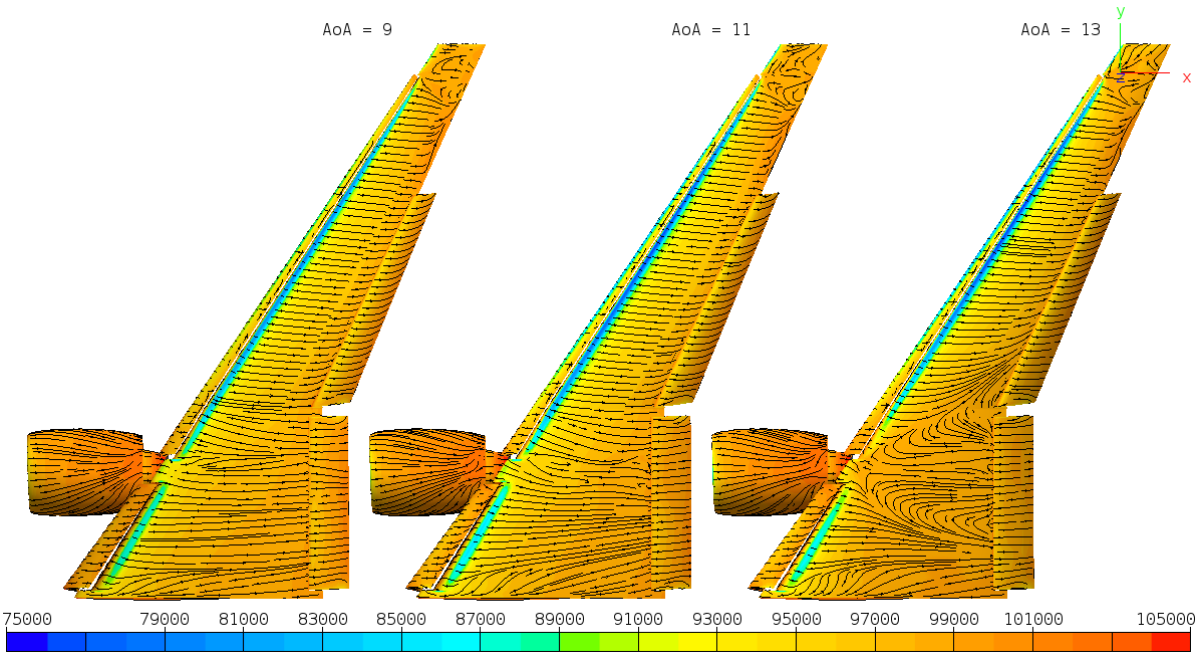

Figure 12: Pressure distribution and skin friction lines on the wing (fully deployed high-lift devices) at Mach=0.25.

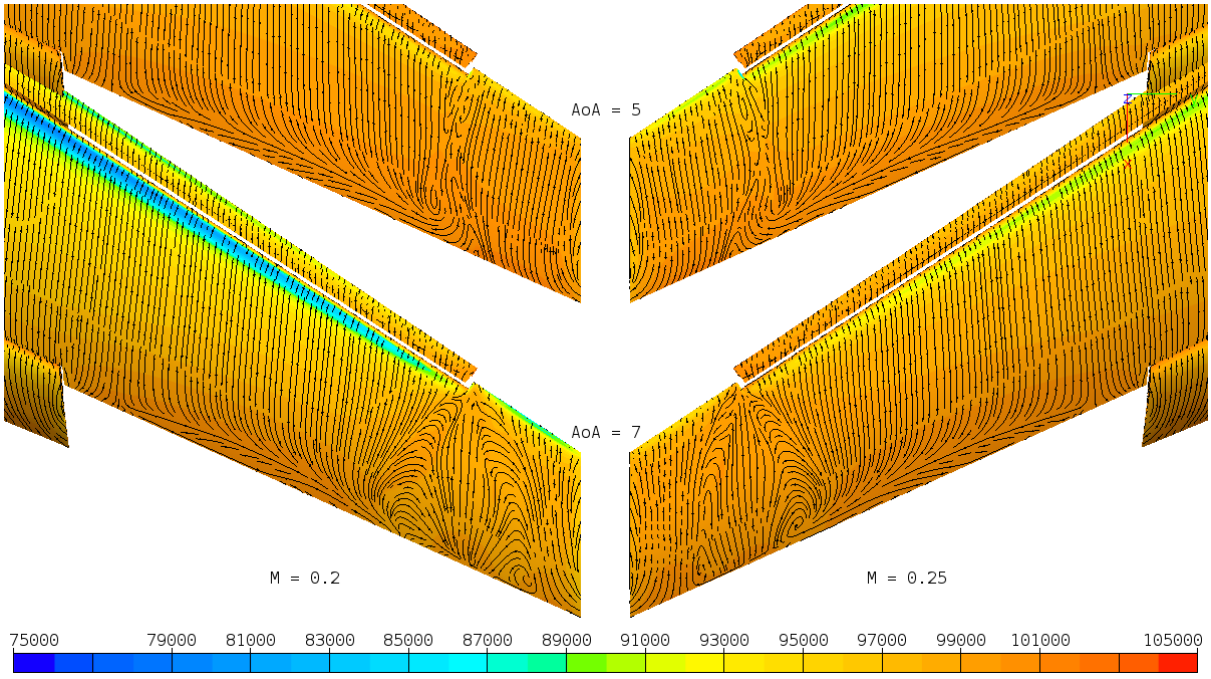

Figure 13: Pressure distribution and skin friction lines on the wing (fully deployed high-lift devices) at Mach=0.20 (left) and Mach=0.25 (right).

6. CONCLUSIONS & FUTURE WORK

Detailed CFD simulations were made for take-off conditions of the DC2 Aircraft designed in the EU funded H2020 AGILE project. The AGILE project is a collaborative project, and the different components of the aircraft (wing/fuselage, engine, pylon/nacelle, high lift system) were provided by different partners in the project. The different aircraft components were merged together to obtain a CAD model that could be used for CFD mesh generation. A multi block structured chimera grid was created to permit quick changes of the deflection angles of the high lift system.

The CFD simulations showed that stall occurs at relatively low angle of attack (between 11^o and 13^o) indicating that the design of the wing and its components (high-lift devices and nacelle/pylon) are not optimal for the take-off conditions. The pylon-wing interaction and the cutting of the slat at this region location can explain the stall anticipation. A flow separation at the wing tip was visible at even lower angles of attack, also a further optimization of the wing including the high-lift system should be made. In particular optimization of the twist distribution, taking into account the wing span loading and stall path behaviour is needed. This was not taken into account in the optimized wing coming from the DC-1 campaign due to the optimization of the clean wing only.

The simulations also showed that the installed thrust might be insufficient at high angle of attack, in particular for Mach numbers above 0.25.

The results of this study will be used to re-evaluate the design of the wing, high-lift system and installed thrust of the DC2 aircraft.

The study presented here shows that it is important to consider take-off conditions early in the aircraft design and optimization process.

ACKNOWLEDGMENTS

The research presented in this paper has been performed in the framework of the AGILE project (Aircraft 3rd Generation MDO for Innovative Collaboration of Heterogeneous Teams of Experts) and has received funding from the European Union Horizon 2020 Programme (H2020-MG-2014-2015) under grant agreement n° 636202. The Swiss participation in the AGILE project was supported by the Swiss State Secretariat for Education, Research and Innovation (SERI) under contract number 15.0162. The authors are grateful to the partners of the AGILE consortium for their contribution and feedback.

REFERENCES

1. Hirschel E.H. CFD - from Solitary Tools to Components of the Virtual Product. Proc. Basel World User CFD Conference in Applied Computational Fluid Dynamics, Freiburg, Germany, May 19 - 23, 1996, pp. 24.1 - 24.9.
2. Hirschel E.H. Towards the Virtual Product in Aircraft Design? Proc. NDF 2000 - Towards a New Fluid Dynamics with its Challenges in Aerospace Engineering. CNRS, Paris, November, 2000. In: Champion M, Periaux J, Pironneau O, Thomas P. (editors). NFD2000: Towards a New Fluid Dynamics. CIMNE Handbooks on Theory and Engineering Applications of Computational Methods, Barcelona 2000.
3. Vos J.B., Rizzi A., Darracq D. and Hirschel E.H. Navier-Stokes solvers in European aircraft design, Progress in Aerospace Sciences, No. 38, 2002.
4. Ciampa P.D. and Nagel B. The AGILE Paradigm: the next generation of collaborative MDO. AIAA 2017-4137, 2017.
5. Lefebvre T., Bartoli N., Dubreuil S., Manzeri M., Lombardi R., Della Vecchi P., Nicolosi F., Ciampa P.D., Anisimov K., Savelyev A. Methodological enhancements in MDO process investigated in the AGILE European Project. AIAA 2017-4140, 2017.
6. Bartoli N., Lefebvre T., Dubreuil S., Olivanti R., Bons N., Martins J.R.R.A., Bouhlel M.-A., Morlier J. An adaptive optimization strategy based on mixture of experts for wing aerodynamic design optimization. AIAA 2017-4433, 2017.
7. Della Vecchia P., Stingo L., Corcione S., Ciliberti D., Nicolosi F., De Marco A. Game Theory and Evolutionary Algorithms applied to MDO in the AGILE European Project. AIAA 2017-4330, 2017.
8. Prakasha P.S. and Ciampa P.D. Airframe-On Board System-Propulsion System Optimization for Regional Transport Aircraft: AGILE EU project CEAS Conference Paper ID-270, 2017.
9. Anisimov K.S. and Savelyev A.A. Aerodynamic Optimization of Airplane Propulsion System within the Framework of AGILE Project 30th ICAS Congress, Daejeon, 2016.

10. Seider D., Fischer P., Litz M., Schreiber A., Gerndt A. Open Source Software Framework for Applications in Aeronautics and Space, IEEE Aerospace Conference, March 2012.
11. DLR, Air Transportation Systems, CPACS Homepage [Online] http://www.cpacs.de, 2017.
12. Neyland V.Y., Bosnyakov S.M., Glazkov S.A., Ivanov A.I., Matyash S.V., Mikhailov S.V. and Vlasenko V.V. Conception of electronic wind tunnel and first results of its implementation Progress in Aerospace Sciences, vol. 37, no. 12, pp. 121-145, 2001.
13. Kurzke J. Performance modeling methodology: Efficiency definitions for cooled single and multistage turbines. ASME 2002-GT-30497, 2002.
14. Kurzke J. Gas Turbine Cycle Design Methodology: A Comparison of Parameter Variation with Numerical Optimization. ASME 98-GT-343, 1998.
15. Vos J.B., Rizzi A.W., Corjon A., Chaput E., Soinne E., Recent Advances in Aerodynamics inside the NSMB (Navier-Stokes Multiblock) Consortium. AIAA paper 98-0225, 1998.
16. Hoarau Y., Pena D., Vos J.B., Charbonnier D., Gehri A., Braza M., Deloze T., Laurendeau E. Recent Developments of the Navier Stokes Multi Block (NSMB) CFD solver. AIAA Paper 2016-2056, 2016.
17. Vos J.B., Charbonnier D., Ludwig T., Merazzi S., Gehri A., Stephani P., Recent Developments on Fluid Structure Interaction in the Navier Stokes Multi Block (NSMB) CFD solver. AIAA Paper 2017-4458, 2017.
18. Langtry, R. and Menter, F. Correlation-based transition modeling for unstructured parallized computational fluid dynamic codes. AIAA Journal, Vol. 47, pp. 2894-2907, 2009.
19. Wakefield I. and Dubuque C. Exceeding Tire Speed Rating during Takeoff. Boeing Aeroquarterly, QTR_02, 2009.